Dalton Transactions

PAPER

View Article Online
View Journal | View Issue

Cite this: *Dalton Trans.*, 2014, **43**, 3589

Micellar self-assemblies of gadolinium(III)/europium(III) amphiphilic complexes as model contrast agents for bimodal imaging†

Elke Debroye,[a] Svetlana V. Eliseeva,[b,c] Sophie Laurent,[d] Luce Vander Elst,[d] Robert N. Muller[d,e] and Tatjana N. Parac-Vogt*[a]

Received 9th October 2013,
Accepted 10th December 2013

DOI: 10.1039/c3dt52842a

www.rsc.org/dalton

The synthesis and characterization of two novel DTPA bisamide derivatives DTPA-BC_{12}PheA and DTPA-BC_{14}PheA functionalized with *p*-dodecylaniline and *p*-tetradecylaniline are described. The ligands were coordinated to Gd(III) and Eu(III), resulting in highly paramagnetic and luminescent complexes, respectively. Mixed micelles consisting of Gd/Eu-DTPA-BC_{12}PheA and DTPA-BC_{14}PheA with a homogeneous size distribution (33–40 nm) were prepared by the assembly of the amphiphilic complexes with phospholipid DPPC and a surfactant Tween 80®. Taking into account the sensitivity difference between magnetic resonance and optical imaging techniques, the ratios of Gd and Eu complexes (Gd/Eu) 1 : 1, 2 : 1, 3 : 1, 20 : 1 and 50 : 1 were combined in one single micelle and their optical and relaxometric properties were characterized in detail. Upon excitation at 290 nm, the micelles display characteristic red emission bands due to the $^5D_0 \rightarrow {}^7F_J$ (J = 0–4) transitions of Eu(III). The number of water molecules in the first coordination sphere of Eu(III) (q_{Eu} = 0.1–0.2) was calculated from the lifetime measurements performed in H_2O and D_2O solutions. Micelles composed of exclusively europium complexes display quantum yields in the range of 1.0%, decreasing with the europium concentration when going from 1 : 1 to 50 : 1 Gd/Eu contents. The ligand-to-lanthanide sensitization efficiency for micelles consisting of Eu-DTPA-BC_{12}PheA and Eu-DTPA-BC_{14}PheA equals 3.8% and 4.1%, respectively. The relaxivity r_1 per Gd(III) ion at 40 MHz and 310 K reaches a maximum value of 14.2 s^{-1} mM^{-1} for the Gd-DTPA-BC_{12}PheA assemblies and 16.0 s^{-1} mM^{-1} for the micellar Gd-DTPA-BC_{14}PheA assemblies compared to a value of 3.5 s^{-1} mM^{-1} for Gd-DTPA (Magnevist®). Theoretical fitting of the ^{1}H NMRD profiles results in τ_R values of 4.2 to 6.6 ns. The optimal concentration ratio of Gd/Eu compounds in the micelles in order to provide the required bimodal performance has been determined to be 20 : 1. In the search for other bimodal systems, this discovery can be used as a guideline concerning the load of paramagnetic agents with respect to luminescent probes.

Introduction

Paramagnetic gadolinium chelates are known to enhance remarkably the longitudinal relaxation rate of water protons, which makes them suitable for magnetic resonance imaging (MRI) applications. Compared to other imaging modalities, MRI provides unique anatomical resolution, but the technique suffers from low sensitivity. To avoid the administration of

[a]*KU Leuven, Department of Chemistry, Celestijnenlaan 200F, 3001 Heverlee, Belgium. E-mail: tatjana.vogt@chem.kuleuven.be; Fax: +32 16 327992; Tel: +32 16 327612*
[b]*Centre de Biophysique Moléculaire CNRS UPR 4301, Rue Charles Sadron, 45071 Orléans Cedex 2, France*
[c]*Le STUDIUM® Institute for Advanced Studies, Orléans and Tours, France*
[d]*University of Mons, Department of General, Organic and Biomedical Chemistry, Place du Parc 23, 7000 Mons, Belgium*
[e]*Center for Microscopy and Molecular Imaging (CMMI), 6041 Gosselies, Belgium*

†Electronic supplementary information (ESI) available: ESI mass spectra of the Eu(III) complexes (Fig. S1), ^{1}H NMR spectra of ligand DTPA-BC_{12}PheA and Eu(III) complexes (Fig. S2), DLS measurements on the assembled micelles (Fig. S3), Relative integral intensities of f–f-transitions for Eu(III) complexes (Table S1), Normalized excitation and absorption spectrum of micelles consisting of Eu-DTPA-BC_{14}PheA (Fig. S4), Relative integral intensities of f–f-transitions for micelles consisting of Eu(III) complexes (Table S2), Photophysical data for micelles consisting of Eu-DTPA-BC_{12}PheA and Eu-DTPA-BC_{14}PheA in water (Table S3), ^{1}H NMRD profiles of micelles composed of Gd/Eu-DTPA-BC_{12}PheA or Gd/Eu-DTPA-BC_{14}PheA complexes compared to Gd-DTPA in water (Fig. S5, S6), fitted by using the Lipari–Szabo model (Fig. S7, S8), Parameters obtained by theoretical fitting of the ^{1}H NMRD data of micelles consisting of Gd/Eu-DTPA-BC_{12}PheA and Gd/Eu-DTPA-BC_{14}PheA (Tables S4 and S5), using the Lipari–Szabo model (Tables S6 and S7). See DOI: 10.1039/c3dt52842a

high concentrations of the MRI agent (0.01–0.1 mM), significant efforts have been made to increase the efficiency per gadolinium unit. For this, the commonly used diethylenetriaminepentaacetic acid (DTPA) or 1,4,7,10-tetraazacyclododecane-1,4,7,10-tetraacetic acid (DOTA) scaffolds are functionalized in order to obtain better structural or dynamic properties. Faster proton relaxivities can be achieved by lengthening the rotational correlation time (τ_R) or shortening the residence time of the coordinated water molecules (τ_M). Already many studies have been performed to optimize this set of parameters.[1–3] The molecular tumbling rate of the contrast agent can be lowered by conjugation of Gd(III) chelates to macromolecules like linear polymers or dendrimers.[2,4–7] Also a non-covalent interaction of the paramagnetic entity with human serum albumin resulted in an amplified proton relaxation.[8–11] Unfortunately, the theoretical maximum efficiency has not yet been reached, since the local motions of the gadolinium complex accompany the slow molecular tumbling of the carrier.[12,13] Another approach to increase the sensitivity is the accumulation of a substantial amount of Gd(III) agents in a small volume. Amphiphilic complexes can be assembled in aqueous solutions forming supramolecular aggregates, like micelles or liposomes.[1,13–16] Their structural properties can easily be tuned by varying the charge of the hydrophilic head-group or the amount and length of hydrophobic side chains.[1] In micelles, the Gd(III) complexes are entirely exposed to the external aqueous surface, providing easy access of the bulk water molecules to the paramagnetic center.

Among the bioimaging techniques, optical imaging is known to possess a low detection limit so that minute concentrations can be perceived. In a recent effort to enhance the imaging performance of contrast agents, probes combining MRI and luminescent activities have been created in order to offer good resolution as well as high sensitivity.[17,18] This approach leads to the same biodistribution of the probe for both techniques, which is advantageous for *in vivo* biological investigations. Several organic dyes have been attached to paramagnetic complexes and their bimodal applications have been exploited.[19–22] In a different approach, transition metal complexes endowed with luminescent properties have been linked to DTPA or DOTA.[23–25] Bimodal agents based on magnetofluorescent liposomes[26,27] and nanoparticles[28–30] have also been reported. Although significant improvements of MRI and optical properties have been achieved, practical applications of aforementioned bio-conjugates are limited by short luminescence lifetimes, a small Stokes shift and poor resistance to photobleaching. During the last decade, lanthanide based systems combining magnetic and optical properties are attracting attention.[31–35] Besides the excited state lifetimes in the range of milliseconds, the lanthanide complexes exhibit very sharp emission bands and an apparent shift between absorption and emission bands. Since the f–f transitions of Ln(III) ions are Laporte forbidden and thus have low molar absorption coefficients, it is necessary to integrate an appropriate chromophore into the coordinated ligand. This will serve as an antenna to capture the incident light and subsequently transfer the energy to the emissive state of the lanthanide ion.

In this report, we present a novel approach towards bimodal contrast agents in which Gd- and Eu-DTPA bisamide complexes functionalized with *p*-dodecylaniline and *p*-tetradecylaniline self-assemble with a saturated phospholipid and a non-ionic surfactant, resulting into micelles with favorable paramagnetic and luminescent properties. Although neutral Gd-DTPA bisamides are generally characterized by a slow water exchange resulting in a larger τ_M value,[1,36,37] a large increase of relaxivity is observed due to the immobilization of the paramagnetic chelate into the micellar membrane.[13,38] On the other hand, the integrated phenyl functions should ensure sensitization of the coordinated luminescent Eu(III) ions, leading to a strong optical signal. Taking into account the different sensitivities of the two imaging modalities, approximately a 100-fold higher concentration of the MRI probe with respect to the optical probe should be administered. In the present case, several ratios of gadolinium *versus* europium complexes are integrated into the micellar systems and the ratio providing the optimal optical and magnetic combination has been experimentally established. The composition of the ligands and of the corresponding Gd(III) and Eu(III) complexes has been confirmed by mass spectrometry, NMR, FT-IR and elemental analysis. The size of the obtained supramolecular micelles has been determined by dynamic light scattering and their luminescent and relaxometric properties have been investigated. It is generally known that the administration of non-ionic gadolinium based contrast agents in patients with advanced renal impairment should be avoided.[39] Nevertheless, during the performed experiments no release of free Gd(III) ions has been observed.

Results and discussion

Synthesis of ligands and complexes

The synthetic pathway towards the ligands consists of two main steps. First, DTPA bisanhydride is formed starting from diethylene triamine pentaacetic acid and acetic anhydride. Afterwards, two equivalents of the hydrophobic aromatic amines *p*-dodecylaniline and *p*-tetradecylaniline are reacted with DTPA bisanhydride leading to DTPA-bis-*p*-dodecylphenyl-amide (DTPA-BC_{12}PheA) and DTPA-bis-*p*-tetradecylphenyl-amide (DTPA-BC_{14}PheA) respectively (Fig. 1). All ligands have been characterized by nuclear magnetic resonance spectroscopy, mass spectrometry, elemental analysis and IR spectroscopy.

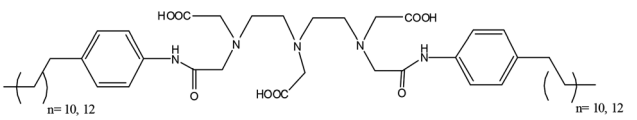

Fig. 1 Chemical structure of DTPA-bis-*p*-dodecylphenyl-amide (n = 10) or DTPA-bis-*p*-tetradecylphenyl-amide (n = 12).

The obtained ligands are coordinated to paramagnetic Gd(III) and to luminescent Eu(III) in pyridine according to a known procedure.[40] The absence of free lanthanide ions is verified by the addition of an arsenazo indicator solution.[41] Molecular peaks $[M + Na]^+$ appear with positive-mode electrospray ionization mass spectrometry (ESI-MS) indicating a 1 : 1 stoichiometry in solution (Fig. S1 in ESI† and Experimental section). Proton NMR spectra of Eu(III)-DTPA-BC_{12}PheA and Eu(III)-DTPA-BC_{14}PheA display broadening of the signals over a large ppm scale (−13 to +32 ppm) due to the paramagnetic nature of europium and an increase of proton resonances in the aliphatic region which is consistent with the occurrence of several interconverting isomers due to the coordination of a lanthanide to a DTPA derivative[42] (Fig. S2 in ESI†). IR spectra of the ligands show strong absorptions in the region around 1600 cm^{-1}, corresponding to the C═O carboxylic acid stretching modes. After complexation, the band shifts by 30 cm^{-1} to lower wavenumbers, which suggests acetate oxygen's coordination to the lanthanide(III) ions. The coordination sphere of the lanthanide is further completed by two carbonyl oxygen atoms of the amide groups and three nitrogen atoms. As a result the complex consists of a hydrophilic center where the DTPA unit implements an eight-fold coordination to the lanthanide ion,[36,37] flanked by two hydrophobic tails which comprise a phenyl group and an aliphatic chain of 12 or 14 carbon atoms. X-ray structures of related DTPA bisamides point out the formation of U-shaped complexes.[43] The lanthanide–water vector is shown to be aligned parallel to the phenyl rings which induces a hydrophobic environment. The long alkyl chains in the *para*-positions create an even more defined hydrophobic area around the lanthanide, hindering water access especially in case of aggregation.

Mixed micelle formation

Due to their amphiphilic nature, the gadolinium and europium complexes of DTPA-BC_{12}PheA and DTPA-BC_{14}PheA could be incorporated into mixed micelles. In this way, the paramagnetic or luminescent agents become an integral part of a supramolecular structure with a decreased rotational motion, targeting a positive contribution to the relaxometric properties. Micelles are formed by mixing 78 mol% phospholipid (DPPC), 15.5 mol% surfactant (Tween 80®) and 6.5 mol% of different ratios of Gd and Eu complexes of each ligand (Gd/Eu = 1 : 1, 2 : 1, 3 : 1, 20 : 1, 50 : 1). The Gd and Eu complexes are combined into one single micelle in order to find a composition with an optimal bimodal performance considering magnetic and optical imaging requirements. The micelle size has been determined by photon correlation spectroscopy at room temperature. Since only one main kind of particle appears in the size distribution profile, the solutions are considered as monodisperse (Fig. S3 in ESI†). As can be seen in Table 1, the mean diameters of the micelles are all within the same range (33–40 nm), which implies that the phospholipid DPPC is the most important factor determining the micelle size.

Table 1 Mean diameters of micelles consisting of DPPC, Tween 80® and Ln-DTPA-BC_{12}PheA or Ln-DTPA-BC_{14}PheA (Ln = Gd/Eu)

Ln(III)-DTPA-BC_{12}PheA	*z*-Average *d* (nm)	Ln(III)-DTPA-BC_{14}PheA	*z*-Average *d* (nm)
Gd/Eu (1 : 1)	37.9	Gd/Eu (1 : 1)	33.1
Gd/Eu (2 : 1)	39.7	Gd/Eu (2 : 1)	39.2
Gd/Eu (3 : 1)	38.3	Gd/Eu (3 : 1)	34.3
Gd/Eu (20 : 1)	35.4	Gd/Eu (20 : 1)	37.1
Gd/Eu (50 : 1)	39.1	Gd/Eu (50 : 1)	36.6

Photophysical properties

Ln(III) complexes. The excitation spectra of Eu-DTPA-bis-*p*-dodecylphenyl-amide and Eu-DTPA-bis-*p*-tetradecylphenyl-amide in a 1 : 1 $CHCl_3$–MeOH mixture are similar and reveal a broad band in the range 240–300 nm with a maximum at ≈265 nm corresponding to the ligand electronic transitions (Fig. 2). In addition, sharp features are seen in the range 360–410 nm, which can be assigned to f–f-transitions of the Eu(III) ion.

Upon excitation into the ligand levels at 290 nm, Eu-DTPA-bis-*p*-dodecylphenyl-amide and Eu-DTPA-bis-*p*-tetradecyl-phenyl-amide exhibit characteristic red luminescence due to $^5D_0 \rightarrow {}^7F_J$ (J = 0–4) transitions. No ligand-centered emission at lower wavelengths is observed indicating that the ligands can efficiently sensitize Eu(III) (Fig. 3). The integral intensities of the hypersensitive $^5D_0 \rightarrow {}^7F_2$ transition, relative to the magnetic dipole $^5D_0 \rightarrow {}^7F_1$ transition, equal 2.3 and 2.4, respectively for Eu-DTPA-BC_{12}PheA and Eu-DTPA-BC_{14}PheA. For each complex, the hypersensitive $^5D_0 \rightarrow {}^7F_2$ transition and $^5D_0 \rightarrow {}^7F_4$ transition have almost equal integral intensities (Table S1 ESI†). The highly forbidden $^5D_0 \rightarrow {}^7F_0$ transition has a quite high intensity, *i.e.* 14–16% relative to the magnetic dipole $^5D_0 \rightarrow {}^7F_1$ transition, which is typical for coordination geometry with C_s, C_n or C_{nv} symmetry.[44]

Luminescence decays of both Eu complexes in a 1 : 1 $CHCl_3$–MeOH mixture have been fitted by mono-exponential equations confirming the presence of only one luminescent lanthanide species in solutions. Luminescence lifetimes are very similar, *i.e.* 0.83-(1) ms and 0.86-(1) ms for Eu-DTPA-BC_{12}PheA and Eu-DTPA-BC_{14}PheA, respectively.

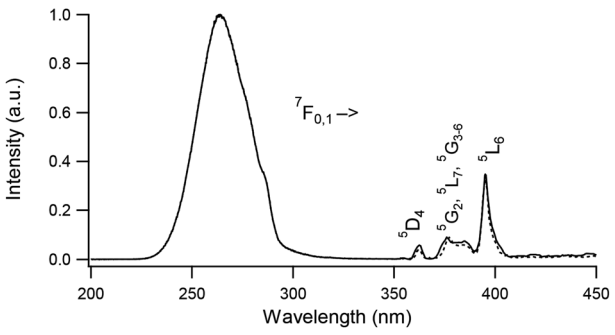

Fig. 2 Normalized excitation spectrum of Eu-DTPA-BC_{12}PheA (dashed trace) and Eu-DTPA-BC_{14}PheA (solid trace) measured while monitoring Eu(III) emission at 614 nm (1 : 1 $CHCl_3$–MeOH, 10^{-4} M, 298 K).

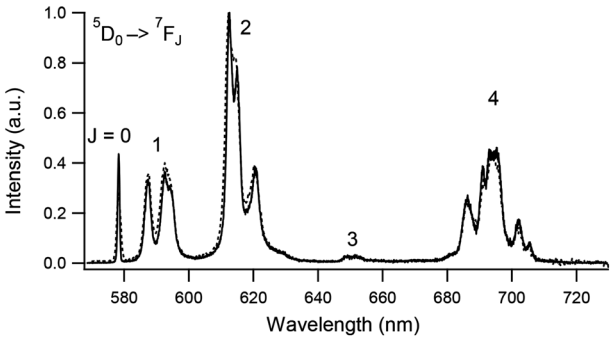

Fig. 3 Corrected and normalized luminescence spectra of Eu-DTPA-BC_{12}PheA (dashed trace) and Eu-DTPA-BC_{14}PheA (solid trace) (1 : 1 $CHCl_3$–MeOH mixture, 10^{-4} M, λ_{exc} = 290 nm, 298 K).

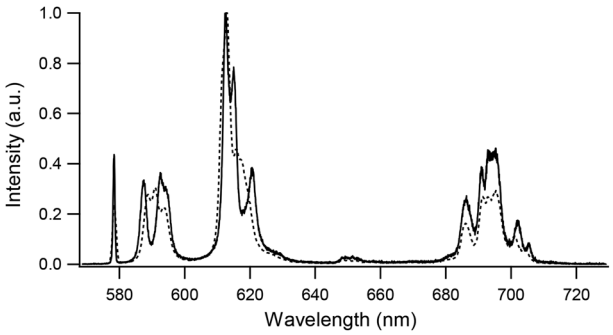

Fig. 5 Corrected and normalized luminescence spectra of Eu-DTPA-BC_{14}PheA (1 : 1 $CHCl_3$–MeOH mixture, solid trace) and micelles consisting of Gd/Eu-DTPA-BC_{14}PheA (H_2O, dashed trace) (10^{-4} M, λ_{exc} = 290 nm, 298 K).

Micelles. After assembly of the Ln(III) complexes with the phospholipid DPPC and surfactant Tween 80®, the excitation spectrum of the micelles exhibit a very similar ligand-centered band in the range 240–300 nm with a maximum at 264 nm. On the other hand, no sharp bands of f–f-transitions of the Eu(III) ion are observed in contrast to the free complexes (Fig. 4).

Upon excitation at 290 nm, the emission spectra display the unique sharp emission bands due to $^5D_0 \rightarrow {}^7F_J$ (J = 0–4) transitions of the Eu(III) ion. The efficient energy transfer from ligand to lanthanide is maintained since no ligand-centered emission is detected. Relative integral intensities of $^5D_0 \rightarrow {}^7F_J$ (J = 0–4) transitions for both Eu(III) micelles (Table S2 ESI†) are the same within experimental errors confirming similarity of the local microenvironment around the lanthanide ions. However, compared to the emission profiles of the complexes which are not incorporated into the micellar structure, the intensity of the $^5D_0 \rightarrow {}^7F_4$ transition decreases by 26–33% while the intensity of the hypersensitive $^5D_0 \rightarrow {}^7F_2$ transition increases by 14–22%. In addition, slight changes in the crystal-field splitting of the f–f transitions are detected (Fig. 5).

All these observations reflect variations in the coordination environment around the Eu(III) ion when going from complexes to micelles. These are induced by a change of solvent ($CHCl_3$–MeOH *vs.* H_2O) and also the influence of the micellar components should not be excluded. The non-ionic surfactant Tween 80® contains hard donor atoms with affinity for the europium ion and is able to form hydrogen bonds with the coordinated water molecule.[45–47]

As can be seen in Fig. 6, the luminescence drops with increasing Gd(III) and decreasing Eu(III) content. A linear relationship between the intensity decreases and the Eu(III) concentration is observed. In Table 2, total integrated intensities of $^5D_0 \rightarrow {}^7F_J$ (J = 0–4) transitions for micelles with decreasing europium contents, relative to micelles composed of exclusively Eu(III) complexes, are represented. The emission of the micelles consisting of Gd/Eu 20 : 1 is still clearly visible, whereas the characteristic red luminescence gradually fades for micelles with less than 1 Eu(III) ion per 20 Gd(III) ions.

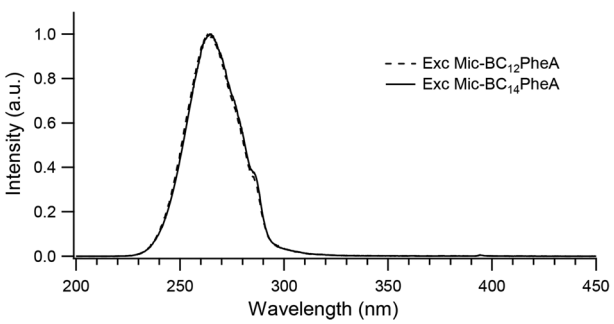

Fig. 4 Normalized excitation spectra of micelles consisting of Eu-DTPA-BC_{12}PheA (dashed trace) and Eu-DTPA-BC_{14}PheA (solid trace) (H_2O, 10^{-4} M, λ_{em} = 614 nm, 298 K).

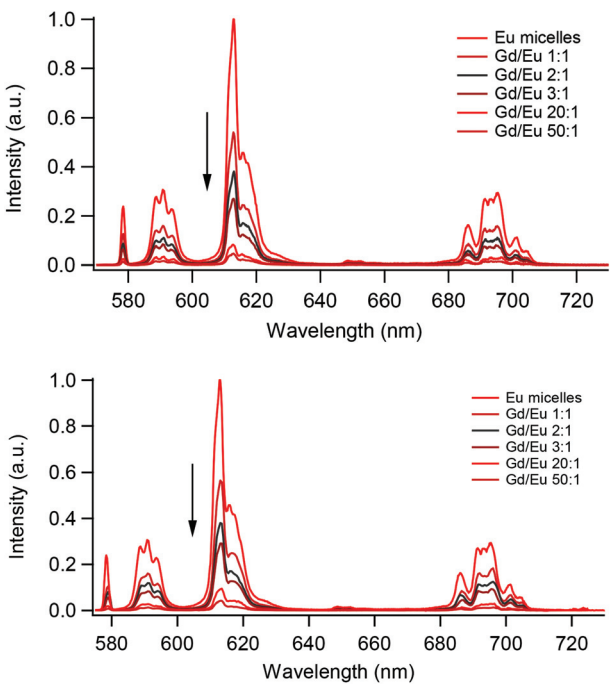

Fig. 6 Corrected and normalized luminescence spectra of micelles consisting of Gd/Eu-DTPA-BC_{12}PheA (top) and Gd/Eu-DTPA-BC_{14}PheA (bottom) (H_2O, 10^{-4} M, λ_{exc} = 290 nm, 298 K).

Table 2 Eu(III) contents relative to micelles composed of exclusively Eu(III) complexes and their corresponding relative total emission intensities (H_2O, 10^{-4} M, λ_{exc} = 290 nm, 298 K)

	Eu(III) content	DTPA-BC_{12}PheA	DTPA-BC_{14}PheA
Gd/Eu (0 : 1)	1.00	1.00	1.00
Gd/Eu (1 : 1)	0.50	0.53	0.56
Gd/Eu (2 : 1)	0.33	0.38	0.38
Gd/Eu (3 : 1)	0.25	0.27	0.29
Gd/Eu (20 : 1)	0.05	0.08	0.09
Gd/Eu (50 : 1)	0.02	0.04	0.04

Luminescence lifetimes in both H_2O and D_2O have been obtained after fitting luminescence decays by mono-exponential equations, which confirm the presence of only one luminescent lanthanide species in the micelles. Luminescence lifetimes in H_2O are equal to 1.36–1.39 (±0.01) ms for both micelles. These τ_{H_2O} values are remarkably high compared to other lanthanide complexes with DTPA bisamide derivatives.[48,49] In D_2O, luminescence lifetimes are prolonged up to 2.19–2.21 (±0.04) ms. Two phenomenological equations developed for cyclen[50] and aminocarboxylate derivatives[51] allow us to determine the number of coordinated water molecules q with an accuracy of ±0.2–0.3 for eqn (1) and ±0.1 for eqn (2):

$$q_{Eu}(H_2O) = 1.2(\Delta k_{obs} - 0.25 - 1.2q^{NH} - 0.075q^{CONH}) \quad (1)$$

$$q_{Eu}(H_2O) = 1.11(\Delta k_{obs} - 0.31 - 0.44q^{OH} - 0.99q^{NH} - 0.075q^{CONH}) \quad (2)$$

Δk_{obs} represents the difference of the decay rate constants $k_{H_2O}(1/\tau_{H_2O})$ and $k_{D_2O}(1/\tau_{D_2O})$ and q^X stands for the number of OH, NH or CONH groups participating in lanthanide coordination. In the present case, only amide groups have been considered, q^{CONH} = 2. After calculation, q_{Eu} values obtained using both equations are in agreement and lie in the range of 0.1–0.2 water molecules. Additionally, luminescence lifetimes upon direct excitation into the europium ion (393 nm, $^7F_{0,1} \leftarrow {}^5L_6$) have been measured and found to be 1.27–1.28 (±0.03) ms in H_2O and 2.02–2.04 (±0.02) ms in D_2O. The corresponding number of coordinated water molecules is calculated to be 0.2. These outcomes are not in agreement with other studied DTPA bisamide complexes in aqueous solutions[52,53] in which the lanthanide ion is eight-fold coordinated while one water molecule is capable of occupying the ninth coordination site. As mentioned before, the non-ionic surfactant at the periphery of the assembled micelles is able to form hydrogen bonds with H_2O and acts as a competitor in lanthanide coordination. Moreover, the complexes possess a defined hydrophobic area in the lanthanide region, further inhibiting water access. Less non-radiative deactivation due to O–H vibrations will take part, leading to longer luminescence lifetimes and as a consequence to a reduced q number found by the phenomenological eqn (1) and (2).

The micelles composed of exclusively europium complexes of DTPA-BC_{12}PheA or DTPA-BC_{14}PheA show a slight difference in Eu(III) quantum yields under ligand excitation (Q^L_{Eu}). Values of 0.98% and 1.10% respectively were obtained. Emission intensity of the micelles (Fig. 6) decreases linearly with increasing Gd/Eu ratio reflecting constancy of quantum yield. Direct excitation of the Eu(III) ion is very inefficient as the relevant f–f transitions are Laporte forbidden, so intrinsic quantum yields (Q^{Eu}_{Eu}) have been estimated according to the following equations comprising the ratio between the observed (τ_{obs}) and radiative (τ_{rad}) lifetimes:

$$\frac{1}{\tau_{rad}} = A_{MD,0} n^3 \left(\frac{I_{tot}}{I_{MD}}\right) \quad (2a)$$

$$Q^{Eu}_{Eu} = \frac{\tau_{obs}}{\tau_{rad}} \quad (2b)$$

The Einstein coefficient $A_{MD,0}$ equals 14.65 s^{-1}, n is the refractive index set equal to that of the neat solvent, n_{H_2O} = 1.34, and (I_{tot}/I_{MD}) represents the ratio of the total integrated $^5D_0 \rightarrow {}^7F_J$ (J = 0–4) emission area to the intensity of the $^5D_0 \rightarrow {}^7F_1$ magnetic dipole (MD) transition. The side chain length of the complexes hardly influences the Q^{Eu}_{Eu} value of the micelles and rather high rates of 26–27% are obtained. This result is in agreement with the former determined elimination of water molecules from the first coordination sphere of the luminescent lanthanide ion. At last, the ratio between the acquired Eu(III) quantum yield under ligand excitation (Q^L_{Eu}) and Eu(III) intrinsic quantum yield (Q^{Eu}_{Eu}) defines the sensitization efficiency (η_{sens}) of the ligand:

$$\eta_{sens} = \frac{Q^L_{Eu}}{Q^{Eu}_{Eu}} \quad (3)$$

resulting in 3.8% for micelles consisting of Eu-DTPA-BC_{12}PheA and 4.1% for micelles consisting of Eu-DTPA-BC_{14}PheA.

Relaxometric studies

Proton NMRD profiles give an idea about the efficiency of a 1 mM solution of Gd(III) agent to shorten the longitudinal relaxation time (T_1) by measuring the water proton relaxivity (r_1) as a function of the magnetic field strength. The relaxation rate is enhanced by dipolar interactions between the gadolinium ion and the proximate water molecules exchanging with bulk water. Besides the inner sphere contribution[54,55] comprising the interactions between Gd(III) and directly coordinated water molecules, also the longer distance interactions with second[56] and outer sphere[57] water molecules, should not be neglected. Inner sphere interactions are defined by several parameters such as the number of water molecules in the first coordination shell (q), the distance between Gd(III) and the water proton nuclei (r), the water residence time (τ_M), the rotational correlation time of the paramagnetic compound (τ_R), the electronic relaxation time of Gd(III) at zero field (τ_{S0}) and the correlation time modulating the electronic relaxation (τ_V). Concerning outer sphere interactions, the distance of closest approach (d) and the relative diffusion coefficient (D) of neighbouring water molecules are also taken into account. For the second sphere contribution, three additional parameters have to be considered: the number of water molecules

in the second hydration sphere (q_{ss}), the distance between the protons of these molecules and the Gd(III) ion (r_{ss}) as well as the correlation time modulating the interaction (τ_{ss}). Although this theoretical model certainly gives a rough description of such complex systems, the proton NMRD profiles of the micelles have been theoretically fitted considering inner sphere, second sphere and outer sphere contributions (Fig. 7). The parameters r, d and r_{ss} are fixed to 0.31, 0.36 and 0.36 nm respectively, D is set to 3.0×10^{-9} m^2 s^{-1} and τ_M is adjusted to 500 ns consistent with other Gd-DTPA bisamide complexes.[35,48,58,59] Since the photophysical study points out that hardly any water molecule is directly bound to the gadolinium ion, the hydration number q is allowed to vary between 0.0 and 0.6, while the number of water molecules in the second coordination shell q_{ss} is allowed to vary between 0.0 and 10.0. The NMRD profiles of the micelles consisting of different ratios of Gd- and Eu-DTPA-BC_{12}PheA in water at 37 °C, all follow the same trend. For clarity, only those with Gd/Eu ratios of 1 : 1 and 50 : 1 are depicted in Fig. 7 in comparison with the data of the clinically administered Gd-DTPA. In a similar way, the NMRD results of micelles consisting of Gd- and Eu-DTPA-BC_{14}PheA are shown. For both assemblies, the different profiles are very similar resulting in comparable parameters obtained by theoretical fitting. An overview of the averaged parameter values for each kind of micelle is displayed in Table 3.

The characteristic maximum for slowly tumbling systems at frequencies between 20 and 60 MHz provides a clear indication for the assembly of the amphiphilic components into supramolecular structures. At 30–40 MHz, r_1-values of 14.2 and 16.0 s^{-1} mM^{-1} per Gd(III) ion have been obtained for the aggregated Gd-DTPA-BC_{12}PheA and Gd-DTPA-BC_{14}PheA complexes respectively. τ_R values of 4.2 to 6.6 ns are obtained, which is in good agreement with the averaged diameter (33–40 nm) of the micelles.[37] The relatively high τ_R values are caused by the anchoring of two aliphatic chains of the paramagnetic chelate into the micellar membrane, leading to a strong reduction of the local motions.[13,38] Although eqn (1) suggests the absence of water molecules in the first coordination sphere of the lanthanide ion, a q_{Gd} of 0.4 to 0.6 is achieved by fitting the proton NMRD profiles. Despite the minimization of the luminescence quenching effect induced by Tween 80®, still a certain amount of coordinated water molecules can be monitored in MR measurements. The modest number of water molecules capable of coordinating to Gd(III) is important for a more efficient relaxation enhancement. Nevertheless, second and outer sphere interactions between water molecules and the paramagnetic center cannot be neglected. The fitting indicates the presence of 2.0–2.5 water molecules in the second coordination shell, which also contributes to the observed relaxivity.

Table 3 Averaged values of the parameters obtained by theoretical fitting of the ^{1}H NMRD profiles of the micelles in water at 37 °C. The fittings and parameters of each kind of micelle are shown in Fig. S5, S6 and in Tables S4, S5

	Micelles DTPA-BC_{12}PheA	Micelles DTPA-BC_{14}PheA
τ_R (ns)	4.2 ± 1.4	6.6 ± 2.4
q	0.40 ± 0.04	0.58 ± 0.04
q_{ss}	2.4 ± 0.5	1.9 ± 0.9
τ_{ss} (ps)	33.4 ± 11.5	25.5 ± 11.0
τ_{SO} (ps)	179 ± 18	121 ± 21
τ_V (ps)	31.0 ± 4.0	24.9 ± 3.4

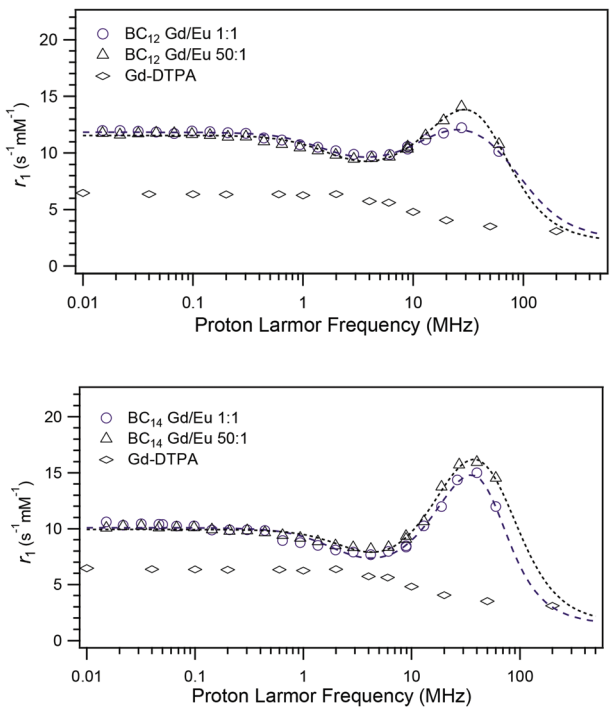

Fig. 7 Proton NMRD profiles of micelles composed of 1 : 1 and 50 : 1 Gd/Eu-DTPA-BC_{12}PheA (top) and of 1 : 1 and 50 : 1 Gd/Eu-DTPA-BC_{14}PheA (bottom) compared to Gd-DTPA in water at 37 °C. The dashed traces represent the fitted data.

Taken into account the formation of supramolecular assemblies, the Lipari–Szabo model has also been used in the analysis of the relaxometric data.[60] In this approach, the hydration number has been fixed to q = 1, neglecting second sphere contributions, r and d are fixed to 0.31 and 0.36 nm respectively, D is set to 3.0×10^{-9} m^2 s^{-1}, τ_M is adjusted to 500 ns and two additional parameters have been introduced. In this model, the global rotational correlation time τ_{RG}, as well as the correlation time governing the local motions τ_{RL}, are considered. Furthermore, the order parameter S^2 describes the internal flexibility where S^2 = 1 stands for a completely rigid system and S^2 = 0 represents a completely flexible system. Fig. 8 depicts the fitted proton NMRD profiles of both kinds of micelles and the corresponding averaged parameter values are displayed in Table 4.

According to the Lipari–Szabo model, the average global correlation time τ_{RG} equals 2.6 and 4.1 ns, while the correlation time governing the local motions τ_{RL} is about 150 and 204 ps, for the BC_{12} and BC_{14} assemblies respectively. Moreover, values of S^2 = 0.15–0.23 for the Gd/Eu-DPTA-BC_{12}PheA micelles and S^2 = 0.30–0.41 for the Gd/Eu-DPTA-BC_{14}PheA micelles have been obtained. The Gd/Eu-DPTA-BC_{14}PheA

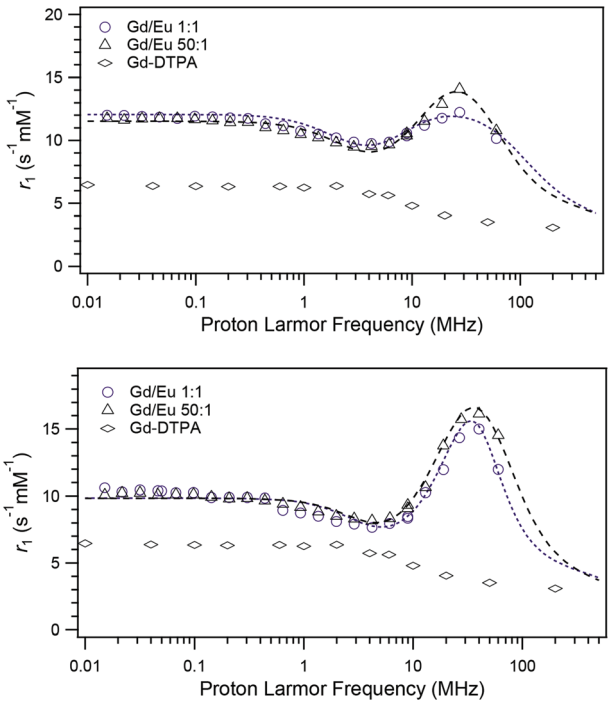

Fig. 8 Proton NMRD profiles of micelles composed of 1 : 1 and 50 : 1 Gd/Eu-DTPA-BC_{12}PheA (top) and of 1 : 1 and 50 : 1 Gd/Eu-DTPA-BC_{14}PheA (bottom) compared to Gd-DTPA in water at 37 °C. The dashed traces represent the fitted data using the Lipari–Szabo model.

Table 4 Averaged values of the parameters obtained by theoretical fitting of the ^{1}H NMRD profiles of the micelles in water at 37 °C using the Lipari–Szabo model. The fittings and parameters of each kind of micelle are shown in Fig. S7, S8 and in Tables S6, S7

	Micelles DTPA-BC_{12}PheA	Micelles DTPA-BC_{14}PheA
q^a	1.0	1.0
τ_{RG} (ns)	2.57 ± 0.65	4.12 ± 1.69
τ_{SO} (ps)	162 ± 28	114 ± 13
τ_V (ps)	44.5 ± 5.0	30.7 ± 2.0
τ_{RL} (ps)	150.0 ± 4.9	203.5 ± 131
S^2	0.20 ± 0.03	0.33 ± 0.04

[a] Fixed value.

complexes clearly display less local flexibility in the supramolecular assemblies due to better insertion into the micellar monolayer leading to a stronger proton relaxation enhancement at frequencies between 20 and 60 MHz.

Some years ago, Kimpe *et al.*[37] prepared mixed micelles consisting of Gd-DTPA-bisamide derivatives with alkyl chains containing 14, 16 and 18 carbon atoms. The micellar compounds with C_{16} chains displayed the best relaxation properties. In Fig. 9, the relaxivities at 20 MHz (0.47 T) and 40 MHz (0.94 T) of the micelles containing Gd-DTPA-BC16, 50 : 1 Gd/Eu-DTPA-BC_{12}PheA and -BC_{14}PheA are compared to the corresponding values of Gd-DTPA.

The relaxivity of the micelles with DTPA-BC_{12}PheA complexes is only slightly higher than that of the DTPA-BC16

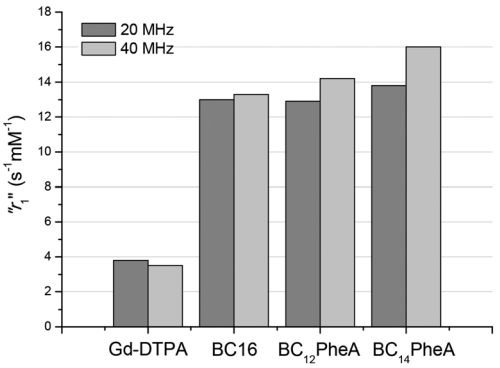

Fig. 9 Relaxivity per Gd for micelles based on Gd-DTPA-BC16, 50 : 1 Gd/Eu-DTPA-BC_{12}PheA and -DTPA-BC_{14}PheA at 20 and 40 MHz.

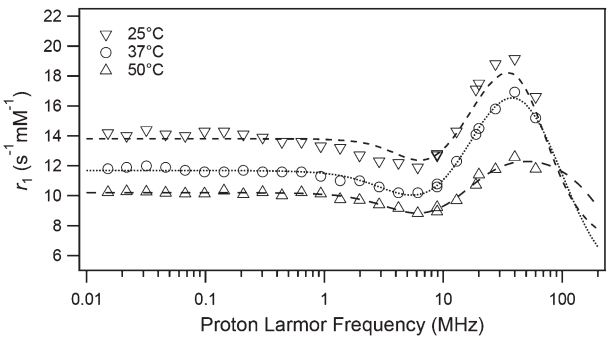

Fig. 10 Proton NMRD profiles of micelles composed of 20 : 1 Gd/Eu-DTPA-BC_{14}PheA in water at 25 °C, 50 °C and 37 °C. The dashed traces represent the fitted data.

analogs. On the other hand, the incorporation of Gd-DTPA-BC_{14}PheA enhances the proton longitudinal relaxation in a more efficient way.

In order to gain more information about the influence of τ_R on the relaxivity enhancement, the NMRD profiles of the 20 : 1 Gd/Eu-DTPA-BC_{14}PheA micelles have also been measured at different temperatures (25 °C and 50 °C) (Fig. 10).

The relaxivity at 40 MHz and 25 °C equals 18.9 s^{-1} mM^{-1}, which is 14 and 52% higher than the relaxivity at 37 and 50 °C respectively. Consequently, we can presume that in the present case the τ_R parameter plays a significant role. Increasing temperature leads to higher molecular motion, resulting in a decrease of proton relaxation efficiency. The profiles have been fitted taking into account inner, second and outer sphere contributions to the paramagnetic relaxation rate. The parameters r, d and r_{ss} are fixed to 0.31, 0.36 and 0.36 nm respectively, D is set to 2.2×10^{-9} m^2 s^{-1} at 25 °C, 3.0×10^{-9} m^2 s^{-1} at 37 °C and 4.0×10^{-9} m^2 s^{-1} at 50 °C. Likewise, τ_M is adjusted to 700 ns at 25 °C, 500 ns at 37 °C and 200 ns at 50 °C. Considering the previous fitting, the hydration number q is fixed to 0.6 and the number of water molecules in the second coordination shell q_{ss} is allowed to vary between 0.0 and 10.0. As can be seen in Table 5, the τ_R value reaches 11.1 ns at 25 °C, while a 3- and 16-fold decrease at 37 °C and 50 °C respectively are observed. Less important, but noteworthy, is the number of water

Table 5 Parameter values obtained by theoretical fitting of the ^{1}H NMRD profiles of micelles consisting of 20 : 1 Gd/Eu-DTPA-BC$_{14}$PheA in water at 25, 37 and 50 °C

	25 °C	37 °C	50 °C
τ_R (ns)	11.1 ± 2.8	3.9 ± 0.6	0.7 ± 0.1
q	0.6	0.6	0.6
q_{ss}	3.8 ± 0.2	3.1 ± 0.1	2.6 ± 0.5
τ_{ss} (ps)	100.0 ± 1.0	44.0 ± 0.8	49.1 ± 5.6
τ_{SO} (ps)	70 ± 3	92 ± 1	81 ± 5
τ_V (ps)	32.0 ± 1.0	28.6 ± 0.8	30.0 ± 2.0
τ_M (ns)	700	500	200

Table 6 Parameter values obtained by theoretical fitting of the ^{1}H NMRD profiles of micelles consisting of 20 : 1 Gd/Eu-DTPA-BC$_{14}$PheA in water at 25, 37 and 50 °C using the Lipari–Szabo model

	25 °C	37 °C	50 °C
τ_{RG} (ns)	3.07 ± 0.56	2.07 ± 0.44	1.42 ± 0.33
τ_{SO} (ps)	165 ± 4	127 ± 4	104 ± 2
τ_V (ps)	29.9 ± 1.0	33.2 ± 1.0	37.7 ± 1.0
τ_{RL} (ps)	667 ± 377	471 ± 129	367 ± 14
S^2	0.64 ± 0.11	0.34 ± 0.09	0.10 ± 0.04
τ_M[a] (ns)	700	500	200

[a] Fixed value.

molecules in the second coordination sphere gradually drops from 3.8 to 2.6, promoting an attenuation of relaxation efficiency. In addition, these observations give an indication about the formation of micelles instead of liposomes. If liposomes had been formed, the increase of the temperature would probably induce an increase of the relaxivity since the exchange of water through the membrane would be faster and the contribution from the complexes in the inner cavity would be increased.[61,62] However, a decrease of the relaxivity is observed when temperature is increased, so rather micellar structures have been obtained.

Fitting by the Lipari–Szabo model for which q has been fixed to 1 also suggests the importance of the τ_R parameter (Fig. 11). At the lower temperature of 25 °C, τ_{RG} is 1.5 to 2.2 times higher compared to the values at 37 and 50 °C, respectively, and the local motions are more restricted. The corresponding fitted parameter values are displayed in Table 6.

Regarding the sizes of the micelles, the DPPC phospholipids and the Gd(III) and Eu(III) complexes, each assembly comprises at least 50 compounds.[1] Since micelles are formed starting from 1 lanthanide complex per 12 DPPC molecules, we can presume the theoretical presence of at least four lanthanide complexes per particle. This leads to the assumption of two Gd(III) complexes per micelle in the 1 : 1 Gd/Eu-DTPA-BC$_n$PheA assemblies, three Gd(III) complexes per micelle in the 3 : 1 Gd/Eu assemblies and approximately four Gd(III) complexes in the 50 : 1 Gd/Eu composition. Per mmol micelle consisting of Gd/Eu-DTPA-BC$_{12}$PheA complexes, relaxation enhancements of maximum 24.8 s^{-1} mM^{-1} for the 1 : 1 Gd/Eu ratio and even 55.3 s^{-1} mM^{-1} for the 50 : 1 Gd/Eu ratio are obtained (Fig. 12). Similarly, the relaxation was enhanced up to 30.0 s^{-1} mM^{-1} and 62.7 s^{-1} mM^{-1} per mmol micelle consisting of Gd/Eu-DTPA-BC$_{14}$PheA complexes.

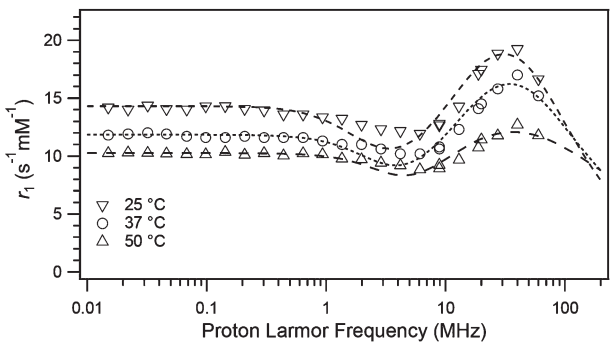

Fig. 11 Proton NMRD profiles of micelles composed of 20 : 1 Gd/Eu-DTPA-BC$_{14}$PheA in water at 25, 37 and 50 °C. The dashed traces represent the fitted data using the Lipari–Szabo approach.

Conclusions

In this study, mixed micelles with a homogeneous size distribution based on amphiphilic DTPA complexes with Gd(III) and

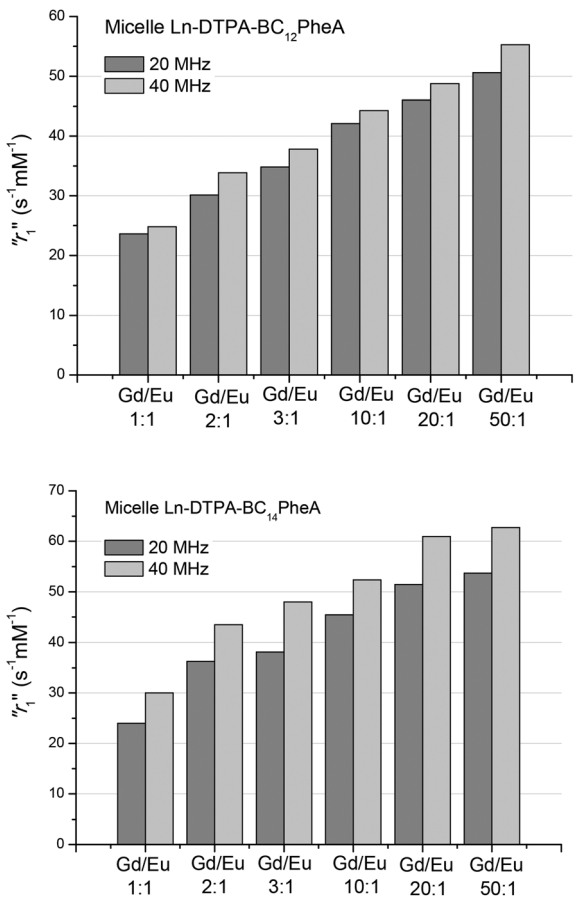

Fig. 12 Relaxation enhancement per mmol micelle based on Gd/Eu-DTPA-BC$_{12}$PheA (top) and Gd/Eu-DTPA-BC$_{14}$PheA (bottom) at 20 and 40 MHz.

Eu(III) were synthesized and evaluated for their magnetic and optical properties. Different ratios of Gd and Eu complexes were combined into one single micelle in order to find the composition with optimal magnetic and optical performance. For all compositions, excitation into the ligand levels at 290 nm resulted in the typical red emission bands due to the $^5D_0 \rightarrow {}^7F_J$ (J = 0–4) transitions of Eu(III). Extremely low q_{Eu} values obtained from the luminescence studies indicate competition between the micelle's non-ionic surfactant and H_2O for coordination to the lanthanide ion. Moreover, the hydrophobic character of the DTPA bisamides prevents easy water access to the coordinated lanthanide ions. The micelles are characterized by a high relaxivity r_1 per Gd(III) ion, reaching a maximum value of 14.2 s^{-1} mM^{-1} for the Gd-DTPA-BC_{12}PheA assemblies and 16.0 s^{-1} mM^{-1} for the micellar Gd-DTPA-BC_{14}PheA at 40 MHz and 310 K. Theoretical fitting of the ^1H NMRD profiles indicates the presence of 0.4 to 0.6 water molecules in the first and 2.0 to 2.5 water molecules in the second coordination sphere. The slow tumbling rate of the micellar systems, the few water molecules capable of coordinating to Gd(III) and the second and outer sphere interactions between water molecules and the paramagnetic center are important for a very efficient relaxation enhancement. The higher relaxivity values for the micelles containing DTPA-BC_{14}PheA complexes is due to restricted local motions because of a more efficient insertion into the lipid monolayer as could be found by fitting the profiles according to the Lipari–Szabo model, fixing q to 1. Temperature dependent relaxivity measurements reveal that τ_R plays a significant role concerning the relaxometric properties of the micelles. Lower temperatures promote the proton relaxation efficiency since the molecular motion of the compound is reduced.

Considering the luminescence spectra and the NMRD profiles of all prepared Gd/Eu micelles and taking into account the sensitivity of the imaging techniques, the optimal ratio of MR *versus* optical reporter in the discussed mixed micelles is determined to be 20 : 1. In these particular systems, the combination of magnetic resonance and optical imaging modalities in one single probe are perfectly compatible. Due to the lack of an integral coordinated inner sphere water molecule, the Eu(III) luminescence suffers less from non-radiative deactivation. Meanwhile, very high relaxivity values are obtained which can be attributed to second and outer sphere interactions and to relatively high τ_R values. Since the sensitivity difference between optical and magnetic resonance imaging is of great importance, these findings can contribute to the development of other model bimodal systems with an optimal load of both imaging probes.

Experimental

Chemicals

Reagents and solvents were obtained from Acros Organics (Geel, Belgium), Sigma-Aldrich (Bornem, Belgium) and BDH Prolabo (Leuven, Belgium), and were used without further purification. Gadolinium(III) chloride hexahydrate was obtained from Alfa Aesar (Ward Hill, USA) and europium(III) chloride hexahydrate was obtained from Acros Organics (Geel, Belgium).

Apparatus and methods

Elemental analysis was performed by using a CE Instruments EA-1110 elemental analyzer. ^1H and ^{13}C NMR spectra were recorded using a Bruker Avance 300 spectrometer (Bruker, Karlsruhe, Germany), operating at 300 MHz for ^1H and 75 MHz for ^{13}C, or on a Bruker Avance 400 spectrometer, operating at 400 MHz for ^1H and 100 MHz for ^{13}C. IR spectra were measured using a Bruker Vertex 70 FT-IR spectrometer (Bruker, Ettlingen, Germany). Mass spectra were obtained using a Thermo Finnigan LCQ Advantage mass spectrometer. Samples for the mass spectrometry were prepared by dissolving the product (2 mg) in methanol (1 mL), then adding 200 μL of this solution to a water–methanol mixture (50 : 50, 800 μL). The resulting solution was injected at a flow rate of 5 μL min^{-1}. The metal contents were detected on a Varian 720-ES ICP optical emission spectrometer with reference to a Chem-Lab gadolinium standard solution (1000 μg mL^{-1}, 2–5% HNO_3). Solutions were dispersed in a 180 W Bandelin Sonorex RK 510 H sonicator equipped with a thermostatic heating bath. Absorption spectra were measured on a Varian Cary 5000 spectrophotometer on freshly prepared aqua solutions in quartz Suprasil® cells (115F-QS) with an optical path-length of 0.2 cm. Emission spectra and luminescence decays of Eu(III) complexes were recorded on an Edinburgh Instruments FS920 steady state spectrofluorimeter. This instrument is equipped with a 450 W xenon arc lamp, a high energy microsecond flashlamp μF900H and an extended red-sensitive photomultiplier (185–1010 nm, Hamamatsu R 2658P). All spectra are corrected for the instrumental functions. Luminescence decays were determined under ligand excitation (290 nm) monitoring emission of the $^5D_0 \rightarrow {}^7F_2$ transition for Eu(III) complexes. Luminescence decays were analyzed using Edinburgh software; lifetimes are averages of at least three measurements. Quantum yields were determined by a comparative method with quinine sulfate (Fluka) in 1 N sulfuric acid (Q = 54.6%) as a standard reference;[63] estimated experimental errors for quantum yield determination ±10%. Solutions with a concentration of about 10^{-5} M were prepared in order to obtain an optical density lower than 0.05 at the excitation wavelength.

Proton NMRD

Proton nuclear magnetic relaxation dispersion (NMRD) profiles were measured on a Stelar Spinmaster FFC, fast field cycling NMR relaxometer (Stelar, Mede (PV), Italy) over a magnetic field strength range extending from 0.24 mT to 0.7 T. Measurements were performed on 0.6 mL samples contained in 10 mm o.d. pyrex tubes. Additional relaxation rates at 20, 60 and 300 MHz were respectively obtained on a Minispec mq20, a Minispec mq60, and a Bruker Avance 300 spectrometer (Bruker, Karlsruhe, Germany). The proton NMRD curves were fitted using data-processing software,[64,65] including

different theoretical models describing the nuclear relaxation phenomena (Minuit, CERN Library).[54,55,57]

DLS measurements

Photon correlation spectroscopy was performed at room temperature with a BIC multiangle laser light scattering system with a 90° scattering angle (Brookhaven Instruments Corporation, Holtsville, USA). The intensity weighted micellar diameter was measured on 1×10^{-4} M diluted suspensions and calculated by a non-negatively constrained least-squares (multiple pass) routine.

DTPA-BC$_{12}$PheA and DTPA-BC$_{14}$PheA according to a slightly modified procedure[37,66]

p-Dodecylaniline (0.52 g, 2 mmol, 2 eq.) or *p*-tetradecylaniline (0.58 g, 2 mmol, 2 eq.) were dissolved in $CHCl_3$ (30 mL). The solution was brought to 40 °C and then added dropwise to a solution of DTPA-bisanhydride (0.36 g, 1 mmol, 1 eq.) in dry DMF (40 mL, 40 °C). The reaction mixture was stirred for eight hours at 50 °C after which the solvents were removed. To the yellowish powder, acetone (20 mL) was added and the suspension was filtered over a Büchner. The pale compound was washed with acetone (2 × 20 mL) and was dried overnight *in vacuo* at 50 °C. The powder was stirred in water (150 mL) at 80 °C for three hours to dissolve excess of DTPA. After filtration, the residue was washed with acetone (2 × 20 mL) again and brought to reflux conditions in 150 mL $CHCl_3$ for another three hours. A creamy white powder was finally obtained after filtration and rinsing with acetone (2 × 20 mL). The pure compound was dried overnight *in vacuo* at 50 °C.

DTPA-BC$_{12}$PheA (0.55 g, 62%) ^{1}H NMR (CD_3OD, 400 MHz): δ (ppm) 0.92 (t, 6H, C**H**$_3$), 1.29 (m, 44H, alkyl C**H**$_2$), 2.06, 2.19 (s, 10H, N–C**H**$_2$–C(O)), 2.91, 2.98, 3.51 (t, 8H, N–C**H**$_2$–C**H**$_2$–N), 7.02 (d, 2H, phenyl C**H**), 7.38 (dd, 4H, phenyl C**H**), 7.54 (d, 2H, phenyl C**H**). ESI-MS in MeOH: *m*/*z* calcd 926.2 $[M + 2Na]^+$ and 949.2 $[M + 3Na]^+$, found 925.6 $[M + 2Na]^+$ and 947.0 $[M + 3Na]^+$. Anal. calcd for $C_{50}H_{81}N_5O_8 \cdot H_2O$: C, 66.86; H, 9.31; N, 7.80; found: C, 66.65; H, 9.78; N, 7.98. FT-IR: ν (cm^{-1}) = 1626 (C═O free acid), 1529 (C═O amide).

DTPA-BC$_{14}$PheA (0.81 g, 86%) ^{1}H NMR (CD_3OD, 400 MHz): δ (ppm) 0.91 (t, 6H, C**H**$_3$), 1.28 (m, 52H, alkyl C**H**$_2$), 2.36, 2.50 (s, 10H, N–C**H**$_2$–C(O)), 2.91, 3.02, 3.56 (t, 8H, N–C**H**$_2$–C**H**$_2$–N), 7.11 (d, 4H, phenyl C**H**), 7.48 (d, 4H, phenyl C**H**). ESI-MS in MeOH: *m*/*z* calcd 937.3 $[M + H]^+$ and 959.3 $[M + Na]^+$, found 938.0 $[M + H]^+$ and 959.4 $[M + Na]^+$. Anal. calcd for $C_{54}H_{89}N_5O_8$: C, 69.27; H, 9.58; N, 7.48; found: C, 69.55; H, 9.65; N, 7.53. FT-IR: ν (cm^{-1}) = 1626 (C═O free acid), 1529 (C═O amide).

Ln(III)-DTPA-BC$_{12}$PheA and Ln(III)-DTPA-BC$_{14}$PheA[37]

The ligand (1 mmol) was dissolved in pyridine (30 mL) and a solution of hydrated $LnCl_3$ salt (1.1 mmol) in H_2O (1 mL) was added. The mixture was brought to 70 °C for 3 hours after which the solvents were evaporated. The crude product was then heated at reflux in ethanol for one hour. The suspension was cooled to room temperature, the complex was filtered off and dried *in vacuo* at 50 °C. The absence of free lanthanide ions was checked with an arsenazo indicator.[41]

^{157}Gd(III)-DTPA-BC$_{12}$PheA. Yield: 68%. ESI-MS in MeOH: *m*/*z* calcd 1057.4 $[M + Na]^+$, found 1057.7 $[M + Na]^+$. Anal. calcd for $C_{50}H_{78}GdN_5O_8 \cdot H_2O$: C, 57.06; H, 7.66; N, 6.65; found: C, 56.77; H, 7.85; N, 6.72. FT-IR: ν (cm^{-1}) = 1595 (COO^- asym. stretch), 1514 (amide II), 1390 (COO^- sym. stretch).

^{152}Eu(III)-DTPA-BC$_{12}$PheA. Yield: 60%. ESI-MS in MeOH: *m*/*z* calcd 1052.2 $[M + Na]^+$, found 1052.0 $[M + Na]^+$. FT-IR: ν (cm^{-1}) = 1595 (COO^- asym. stretch), 1514 (amide II), 1390 (COO^- sym. stretch).

^{157}Gd(III)-DTPA-BC$_{14}$PheA. Yield: 79%. ESI-MS in MeOH: *m*/*z* calcd 1113.5 $[M + Na]^+$, found 1112.8 $[M + Na]^+$. Anal. calcd for $C_{54}H_{86}GdN_5O_8 \cdot H_2O$: C, 58.51; H, 8.00; N, 6.32; found: C, 58.08; H, 8.34; N, 6.37. FT-IR: ν (cm^{-1}) = 1595 (COO^- asym. stretch), 1514 (amide II), 1392 (COO^- sym. stretch).

^{152}Eu(III)-DTPA-BC$_{14}$PheA. Yield: 80%. ESI-MS in MeOH: *m*/*z* calcd 1108.3 $[M + Na]^+$, found 1108.4 $[M + Na]^+$. FT-IR: ν (cm^{-1}) = 1595 (COO^- asym. stretch), 1514 (amide II), 1392 (COO^- sym. stretch).

Preparation of micelles[37]

1,2-Dipalmitoyl-*sn*-glycero-3-phosphocholine (DPPC, 225 mg, 0.3 mmol, 12 eq.) and the amphiphilic complex (25 mg, ±0.025 mmol, 1 eq.) were dissolved in 50 mL of a 1 : 1 chloroform–methanol solution. After evaporation of the solvents, a thin film was obtained which was rehydrated with 5 mL of hot water (70 °C). To improve the solubility, the suspension was sonicated in a 180 W sonicator with a thermostatic bath at 65 °C for 15 min. Polyoxyethylene sorbitan monooleate or Tween 80® (75 mg, 0.06 mmol, 2.4 eq.) was added as a surfactant followed by another 15 minutes of sonication to fulfill the process of micelle formation. Water was evaporated while slowly reducing pressure.

Micelles were obtained by assembling different ratios of gadolinium and europium complexes of DTPA-BC$_n$PheA with n = 12 or 14. The ratios Gd/Eu equaled 0 : 1, 1 : 1, 2 : 1, 3 : 1, 10 : 1, 20 : 1, 50 : 1.

Acknowledgements

E.D. and T.N.P.V. acknowledge the IWT Flanders (Belgium) and the FWO Flanders (project G.0412.09) for financial support. S.V.E. was a visiting postdoctoral fellow of the FWO Flanders (project G.0412.09) and now works at the Centre de Biophysique Moléculaire – CNRS in Orléans. S.V.E thanks the French National Research Agency (Project ANR-10-BLAN-1513). CHN microanalysis was performed by Mr Dirk Henot. ESI-MS measurements were done by Mr Dirk Henot and Mr Bert Demarsin and ICP-OES measurements were performed by Ms. Elvira Vassilieva (Department of Earth and Environmental Sciences). Mr Karel Duerinckx is acknowledged for his help with the NMR measurements. S.L., L.V.E. and R.N.M. thank the ARC Programs of the French Community of Belgium, the FNRS (Fonds National de la Recherche Scientifique), the

support and sponsorship concerted by COST Actions (D38 and TD1004), the EMIL and ENCITE programs and the Center for Microscopy and Molecular Imaging (CMMI, supported by the European Regional Development Fund and the Walloon Region).

Notes and references

1 A. Accardo, D. Tesauro, L. Aloj, C. Pedone and G. Morelli, *Coord. Chem. Rev.*, 2009, **253**, 2193–2213.
2 A. J. L. Villaraza, A. Bumb and M. W. Brechbiel, *Chem. Rev.*, 2010, **110**, 2921–2959.
3 S. Viswanathan, Z. Kovacs, K. N. Green, S. J. Ratnakar and A. D. Sherry, *Chem. Rev.*, 2010, **110**, 2960–3018.
4 P. Lebdušková, J. Kotek, P. Hermann, L. Vander Elst, R. N. Muller, I. Lukeš and J. A. Peters, *Bioconjugate Chem.*, 2004, **15**, 881–889.
5 C.-H. Huang, K. Nwe, A. Al Zaki, M. W. Brechbiel and A. Tsourkas, *ACS Nano*, 2012, **6**, 9416–9424.
6 Y. Li, M. Beija, S. Laurent, L. Vander Elst, R. N. Muller, H. T. T. Duong, A. B. Lowe, T. P. Davis and C. Boyer, *Macromolecules*, 2012, **45**, 4196–4204.
7 K. Luo, G. Liu, W. She, Q. Wang, G. Wang, B. He, H. Ai, Q. Gong, B. Song and Z. Gu, *Biomaterials*, 2011, **32**, 7951–7960.
8 M. Zhen, J. Zheng, L. Ye, S. Li, C. Jin, K. Li, D. Qiu, H. Han, C. Shu, Y. Yang and C. Wang, *ACS Appl. Mater. Interfaces*, 2012, **4**, 3724–3729.
9 T. N. Parac-Vogt, K. Kimpe, S. Laurent, L. Vander Elst, C. Burtea, F. Chen, R. N. Muller, Y. Ni, A. Verbruggen and K. Binnemans, *Chem.–Eur. J.*, 2005, **11**, 3077–3086.
10 P. Caravan, *Acc. Chem. Res.*, 2009, **42**, 851–862.
11 C. Henoumont, V. Henrotte, S. Laurent, L. Vander Elst and R. N. Muller, *J. Inorg. Biochem.*, 2008, **102**, 721–730.
12 S. Aime, D. D. Castelli, S. G. Crich, E. Gianolio and E. Terreno, *Acc. Chem. Res.*, 2009, **42**, 822–831.
13 F. Kielar, L. Tei, E. Terreno and M. Botta, *J. Am. Chem. Soc.*, 2010, **132**, 7836–7837.
14 T. N. Parac-Vogt, K. Kimpe, S. Laurent, C. Piérart, L. Vander Elst, R. N. Muller and K. Binnemans, *Eur. J. Inorg. Chem.*, 2004, 3538–3543.
15 E. Terreno, D. Delli Castelli, C. Cabella, W. Dastrù, A. Sanino, J. Stancanello, L. Tei and S. Aime, *Chem. Biodiversity*, 2008, **5**, 1901–1912.
16 C. Vanasschen, N. Bouslimani, D. Thonon and J. F. Desreux, *Inorg. Chem.*, 2011, **50**, 8946–8958.
17 A. Louie, *Chem. Rev.*, 2010, **110**, 3146–3195.
18 L. Frullano and T. J. Meade, *J. Biol. Inorg. Chem.*, 2007, **12**, 939–949.
19 L. Josephson, M. F. Kircher, U. Mahmood, Y. Tang and R. Weissleder, *Bioconjugate Chem.*, 2002, **13**, 554–560.
20 J. Kuil, T. Buckle, H. Yuan, N. S. van den Berg, S. Oishi, N. Fujii, L. Josephson and F. W. B. van Leeuwen, *Bioconjugate Chem.*, 2011, **22**, 859–864.
21 A. Keliris, T. Ziegler, R. Mishra, R. Pohmann, M. G. Sauer, K. Ugurbil and J. Engelmann, *Bioorg. Med. Chem.*, 2011, **19**, 2529–2540.
22 W. Di, S. K. P. Velu, A. Lascialfari, C. Liu, N. Pinna, P. Arosio, Y. Sakka and W. Qin, *J. Mater. Chem.*, 2012, **22**, 20641–20648.
23 G. Dehaen, S. V. Eliseeva, K. Kimpe, S. Laurent, L. Vander Elst, R. N. Muller, W. Dehaen, K. Binnemans and T. N. Parac-Vogt, *Chem.–Eur. J.*, 2012, **18**, 293–302.
24 G. Dehaen, S. V. Eliseeva, P. Verwilst, S. Laurent, L. Vander Elst, R. N. Muller, W. De Borggraeve, K. Binnemans and T. N. Parac-Vogt, *Inorg. Chem.*, 2012, **51**, 8775–8783.
25 E. Debroye, G. Dehaen, S. V. Eliseeva, S. Laurent, L. Vander Elst, R. N. Muller, K. Binnemans and T. N. Parac-Vogt, *Dalton Trans.*, 2012, **41**, 10549–10556.
26 N. Kamaly, T. Kalber, G. Kenny, J. Bell, M. Jorgensen and A. Miller, *Org. Biomol. Chem.*, 2010, **8**, 201–211.
27 S. J. Soenen, G. V. Velde, A. Ketkar-Atre, U. Himmelreich and M. De Cuyper, *Wiley Interdiscip. Rev.: Nanomed. Nanobiotechnol.*, 2011, **3**, 197–211.
28 W. J. Rieter, J. S. Kim, K. M. L. Taylor, H. An, W. Lin, T. Tarrant and W. Lin, *Angew. Chem. Int. Ed*, 2007, 46, 3680–3682.
29 P. Howes, M. Green, A. Bowers, D. Parker, G. Varma, M. Kallumadil, M. Hughes, A. Warley, A. Brain and R. Botnar, *J. Am. Chem. Soc.*, 2010, **132**, 9833–9842.
30 S. Ronchi, M. Colombo, P. Verderio, S. Mazzucchelli, F. Corsi, C. De Palma, R. Allevi, E. Clementi and D. Prosperi, *AIP Conference Proceedings*, 2010, **1275**, 102–105.
31 F. A. Rojas-Quijano, E. T. Benyó, G. Tircsó, F. K. Kálmán, Z. Baranyai, S. Aime, A. D. Sherry and Z. Kovács, *Chem.–Eur. J.*, 2009, **15**, 13188–13200.
32 G. Tallec, P. H. Fries, D. Imbert and M. Mazzanti, *Inorg. Chem.*, 2011, **50**, 7943–7945.
33 C. S. Bonnet, F. Buron, F. Caillé, C. M. Shade, B. Drahoš, L. Pellegatti, J. Zhang, S. Villette, L. Helm, C. Pichon, F. Suzenet, S. Petoud and É. Tóth, *Chem.–Eur. J.*, 2012, **18**, 1419–1431.
34 S. L. C. Pinho, H. Faneca, C. F. G. C. Geraldes, J. Rocha, L. D. Carlos and M.-H. Delville, *Eur. J. Inorg. Chem.*, 2012, **2012**, 2828–2837.
35 E. Debroye, S. V. Eliseeva, S. Laurent, L. Vander Elst, S. Petoud, R. N. Muller and T. N. Parac-Vogt, *Eur. J. Inorg. Chem.*, 2013, **2013**, 2629–2639.
36 W. J. M. Mulder, G. J. Strijkers, G. A. F. van Tilborg, A. W. Griffioen and K. Nicolay, *NMR Biomed.*, 2006, **19**, 142–164.
37 K. Kimpe, T. N. Parac-Vogt, S. Laurent, C. Piérart, L. Vander Elst, R. N. Muller and K. Binnemans, *Eur. J. Inorg. Chem.*, 2003, **2003**, 3021–3027.
38 Z. Zhang, M. T. Greenfield, M. Spiller, T. J. McMurry, R. B. Lauffer and P. Caravan, *Angew. Chem., Int. Ed.*, 2005, 44, 6766–6769.
39 S. K. Morcos, *Br. J. Radiol.*, 2007, **80**, 73–76.

40 S. Laurent, T. N. Parac-Vogt, K. Kimpe, C. Thirifays, K. Binnemans, R. N. Muller and L. Vander Elst, *Eur. J. Inorg. Chem.*, 2007, **2007**, 2061–2067.
41 H. Onishi and K. Sekine, *Talanta*, 1972, **19**, 473–478.
42 C. Geraldes, A. M. Urbano, M. A. Hoefnagel and J. A. Peters, *Inorg. Chem.*, 1993, **32**, 2426–2432.
43 D. Parker, K. Pulukkody, F. C. Smith, A. Batsanov and J. A. K. Howard, *J. Chem. Soc., Dalton Trans.*, 1994, 689–693.
44 J.-C. Bünzli and S. V. Eliseeva, in *Lanthanide Luminescence*, ed. P. Hänninen and H. Härmä, Springer, Berlin, Heidelberg, 2011, vol. 7, pp. 1–45.
45 I. Hemmilä, S. Dakubu, V.-M. Mukkala, H. Siitari and T. Lövgren, *Anal. Biochem.*, 1984, **137**, 335–343.
46 I. Hemmilá and V.-M. Mukkala, *Crit. Rev. Clin. Lab. Sci.*, 2001, **38**, 441–519.
47 J. A. Keelan, J. T. France and P. M. Barling, *Clin. Chem.*, 1987, **33**, 2292–2295.
48 G. Dehaen, P. Verwilst, S. V. Eliseeva, S. Laurent, L. Vander Elst, R. N. Muller, W. M. De Borggraeve, K. Binnemans and T. N. Parac-Vogt, *Inorg. Chem.*, 2011, **50**, 10005–10014.
49 J. M. Couchet, J. Azéma, C. Galaup and C. Picard, *J. Lumin.*, 2011, **131**, 2735–2745.
50 A. Beeby, I. M. Clarkson, R. S. Dickins, S. Faulkner, D. Parker, L. Royle, A. S. de Sousa, J. A. Gareth Williams and M. Woods, *J. Chem. Soc., Perkin Trans. 2*, 1999, 493–504.
51 R. M. Supkowski and W. D. Horrocks Jr., *Inorg. Chim. Acta*, 2002, **340**, 44–48.
52 S. Aime, F. Benetollo, G. Bombieri, S. Colla, M. Fasano and S. Paoletti, *Inorg. Chim. Acta*, 1997, **254**, 63–70.
53 Y.-M. Wang, Y.-J. Wang, R.-S. Sheu, G.-C. Liu, W.-C. Lin and J.-H. Liao, *Polyhedron*, 1999, **18**, 1147–1152.
54 I. Solomon, *Phys. Rev.*, 1955, **99**, 559–565.
55 N. Bloembergen, *J. Chem. Phys.*, 1957, **27**, 572–573.
56 M. Botta, *Eur. J. Inorg. Chem.*, 2000, **2000**, 399–407.
57 J. H. Freed, *J. Chem. Phys.*, 1978, **68**, 4034–4037.
58 S. Laurent, L. Vander Elst, F. Botteman and R. Muller, *Eur. J. Inorg. Chem.*, 2008, **2008**, 4369–4379.
59 L. Vander Elst, A. Sessoye, S. Laurent and R. N. Muller, *Helv. Chim. Acta*, 2005, **88**, 574–587.
60 G. Lipari and A. Szabo, *J. Am. Chem. Soc.*, 1982, **104**, 4546–4559.
61 S. Hak, H. M. H. F. Sanders, P. Agrawal, S. Langereis, H. Grüll, H. M. Keizer, F. Arena, E. Terreno, G. J. Strijkers and K. Nicolay, *Eur. J. Pharm. Biopharm.*, 2009, **72**, 397–404.
62 G. J. Strijkers, W. J. M. Mulder, R. B. van Heeswijk, P. M. Frederik, P. Bomans, P. C. M. M. Magusin and K. Nicolay, *MAGMA*, 2005, **18**, 186–192.
63 D. F. Eaton, *Pure Appl. Chem.*, 1988, **60**, 1107–1114.
64 R. N. Muller, D. Declercq, P. Vallet, F. Giberto, B. Daminet, H. W. Fischer, F. Maton and Y. Van Haverbeke, ESMRMB, 7th Annual Congress, Strasbourg, 1990.
65 P. Vallet, PhD Dissertation, University of Mons-Hainaut, Belgium, 1992.
66 F. Jasanada and F. Nepveu, *Tetrahedron Lett.*, 1992, **33**, 5745–5748.